A Charge-Orbital Balance Picture of Doping in Colloidal Quantum Dot Solids

Oleksandr Voznyy,[†] David Zhitomirsky,[†] Philipp Stadler, Zhijun Ning, Sjoerd Hoogland, and Edward H. Sargent*

Department of Electrical and Computer Engineering, University of Toronto, 10 King's College Road, Toronto, Ontario, M5S 3G4, Canada. [†]These authors contributed equally to this work.

ABSTRACT

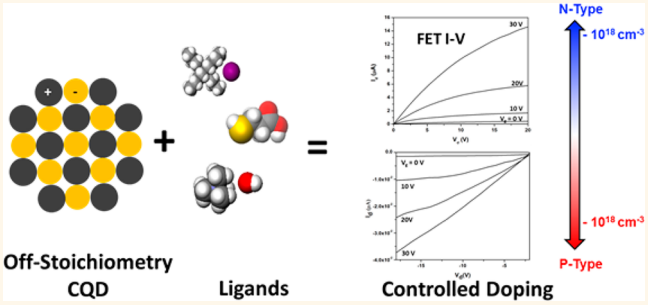

We present a framework—validated using both modeling and experiment—to predict doping in CQD films. In the ionic semiconductors widely deployed in CQD films, the framework reduces to a simple accounting of the contributions of the oxidation state of each constituent, including both inorganic species and organic ligands. We use density functional theory simulations to confirm that the type of doping can be reliably predicted based on the overall stoichiometry of the CQDs, largely independent of microscopic geometrical bonding configurations. Studies employing field-effect transistors constructed from CQDs that have undergone various chemical treatments, coupled with Rutherford backscattering and X-ray photoelectron spectroscopy to provide compositional analysis, allow us to test and confirm the proposed model in an experimental framework. We investigate both p- and n-type electronic doping spanning a wide range of carrier concentrations from 10^{16} cm^{-3} to over 10^{18} cm^{-3}, and demonstrate reversible switching between p- and n-type doping by changing the CQD stoichiometry. We show that the summation of the contributions from all cations and anions within the film can be used to predict accurately the majority carrier type. The findings enable predictable control over majority carrier concentration *via* tuning of the overall stoichiometry.

KEYWORDS: doping · colloidal quantum dots · PbS nanocrystals · DFT · FET · RBS

Thin films based on colloidal quantum dots (CQD) are attractive for optoelectronic devices due to the size-effect tunability of their bandgap combined with large-area room-temperature materials processing. Quantum dots made using binary ionic compound semiconductors such as PbS, CdS, PbSe, CdSe, and InAs, as well as, recently, ternaries such as PbS_xSe_{1-x}, have seen particular application in optoelectronics including electroluminescent devices, photodetectors, and solar cells.[1−6]

Control over free carrier density—both doping type (p-type *vs* n-type) and magnitude—is a crucial degree of freedom in electronic and optical device engineering.[7−9] To date, rectifying devices based on colloidal quantum dots have employed a single type of CQD (usually p-type) with the rectifying junction formed as a heterojunction with a bulk material, such as n-type TiO_2.[1] It would be attractive in applications ranging from solar photovoltaics to lighting and lasing to have the dexterity to vary widely the doping type and magnitude using quantum-tuned solids: advanced optoelectronic devices such as p−n−p bipolar transistors, p−n−p−n thyristors, and multijunction devices enabled by heavily doped tunnel junctions would all become manufacturable entirely *via* solution-processing with the advent of such wide-ranging doping control.

Specific approaches to doping of nanocrystals have been demonstrated in a number of materials systems. PbSe CQDs were shown to demonstrate either n-type or p-type behavior through a careful control of their exposure to hydrazine and ambient air.[10] CdSe was p-doped with the use of silver ions[11] and n-doped by indium infusion,[12] the use of sodium biphenyl as a remote dopant,[13] and metal cations.[14,15] In InAs, n-type doping was accomplished through Cd incorporation,[3] while n-, intrinsic and p-type behaviors were achieved by inclusion of same-valency copper, gold, and silver ions, respectively.[16] Electrochemical doping has also been used in nanocrystalline HgTe[17] and CdSe films[11] to control the carrier populations in the CQDs *via* their exposure to cations or anions from solution.

* Address correspondence to ted.sargent@utoronto.ca.

Received for review July 26, 2012 and accepted August 28, 2012.

Published online August 28, 2012
10.1021/nn303364d

Intrinsic character in PbS CQD films has been achieved by using dithiol ligands.[18] Prior reports suggest that the doping type strongly depends on the geometry of dopant incorporation (surface or core, substitution, or interstitial); however, despite significant efforts aimed at accurate quantification of doping sites and levels, the resulting majority carrier type has not been systematically predictable, and the doping mechanism remains incompletely understood for each particular case.

Here we propose a generalized doping framework based on charge-orbital balance analysis. Our aim is to develop a doping model capable of both predicting the type of doping and its magnitude, applicable to a wide range of CQD systems. In this picture, doping type is a function of the precise composition of the CQDs (*i.e.*, stoichiometry), whereas it is largely insensitive to the microscopic geometrical configurations of the dopants and nanoparticles. In sum, the charge−orbital balance analysis leads to a simple accounting procedure that totals up positive and negative ionic contributions and evaluates the sign and magnitude, leading directly to a prediction of doping type and level. This ultimately reduces to a straightforward analysis of the total stoichiometry of the CQD film.

In this work, we test and confirm this picture using theoretical modeling of PbS CQDs with a variety of stoichiometries and ligands. We then verify the simulations experimentally by varying stoichiometry through synthesis or ligand treatment, monitoring stoichiometry using Rutherford backscattering (RBS) and X-ray photoelectron spectroscopy (XPS), and then measuring net doping using field-effect transistor (FET) test structures. Finally, we show experimentally how the doping can be reversibly switched between n-type and p-type by modulating the stoichiometry within a single film through alteration of oxygen incorporation.

RESULTS AND DISCUSSION

Charge−Orbital Balance Model. Our generalized picture of doping will begin with determining the number of valence electrons available in the system and comparing it with the number of orbitals in the valence shell that are available for filling using said valence electrons. We write the number of excess electrons in the system:

$$N_{\mathrm{exc}} = \sum_{\mathrm{atoms}} N_{\mathrm{e}}^{\mathrm{atom}} - N_{\mathrm{orb}}^{\mathrm{QD}} \qquad (1)$$

where $N_{\mathrm{e}}^{\mathrm{atom}}$ represents the valence electrons counted on a per atom basis, while the number of available orbitals, $N_{\mathrm{orb}}^{\mathrm{QD}}$, is a property of the system as a whole and will be evaluated in detail below. Complete filling of the valence orbitals ($N_{\mathrm{exc}} = 0$) corresponds to a closed electronic shell configuration and results in an intrinsic material. An excess of electrons ($N_{\mathrm{exc}} > 0$) populates the conduction band and results in n-type doping, while a paucity of electrons and incomplete filling of the valence band ($N_{\mathrm{exc}} < 0$) results in p-type doping.

To compute the number of orbitals of the system we follow valence bond theory,[19] which uses atomic orbitals of the isolated atoms as its mathematical basis. It should be noted that atomic orbitals filled in isolated atoms would not necessarily be filled in the final system. For example, in isolated atoms, the topmost filled p-shell in Pb or s-shell in Cd contains 2 electrons; however, these electrons would be transferred to the more electronegative anions in the final system, such as S in the case of PbS. The above-mentioned shells become empty and form the conduction band of the CQD (S1). Such microscopic details about the electronic structure are generally known from literature[20,21] or from calculations for a bulk material.

In covalent systems (*e.g.*, elementary semiconductors), the interaction between atomic orbitals and their splitting into bonding and antibonding states has to be taken into account,[22] leading to the requirement of counting the bonds and thus simplifying the general model to charge−bond balance, widely employed to describe doping in bulk semiconductors.[23] In small nanoclusters this bond-counting still remains valid, although, in light of the increase of the bandgap due to quantum confinement, the dopant energy levels may manifest within the bandgap.[24,25]

Simplified Model for Ionic Crystals. In ionic CQD systems (practically most binary compounds), it is sufficient to count the atomic orbitals contributing to the final valence orbitals of the CQD on a per atom basis. As a rule of thumb, filling of the atomic orbitals in the final system reflects the closed electronic shell condition for each atom, thus, the excess of electrons contributed by each atom is directly related to its oxidation state, which can be positive or negative.

Grouping the same chemical species of atoms and molecules in an ionic CQD system and assigning them an oxidation state, allows us to simplify eq 1 to the following:

$$N_{\mathrm{exc}} = \sum_i N_i q_i \qquad (2)$$

where N_i is the number of species of type i composing a CQD and q_i is their oxidation state. Stable molecular units such as surface ligands are counted using a single oxidation state, such as −1 for monovalent oleate ($RCOO^-$) or thiolate (RS^-) ligands. Charge-neutral ligands that are bound datively, often called L-type ligands, such as amines or trioctylphosphine oxide, make no net contribution in the charge-orbital balance picture, although they may slightly shift the energy of the levels within the system.[26] The choice of oxidation state for a particular atomic species should reflect its most stable configuration within the host material system. Once it is known, our empirical scheme can be used. In some cases, second order effects may cause

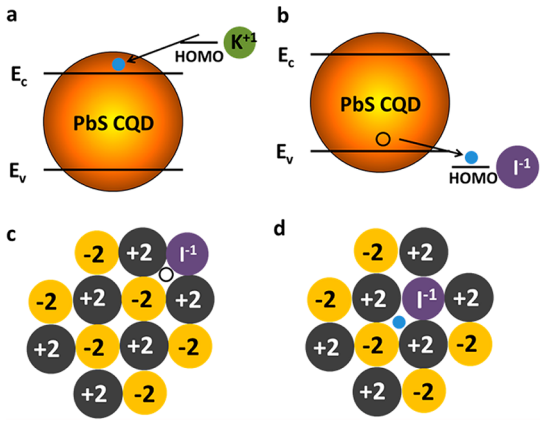

Figure 1. (a) Electron transfer from a remote cation (potassium) HOMO to a CQD conduction band, leading to n-type behavior; (b) transfer of electron from a CQD valence band to a remote anion (iodide) HOMO leading to p-type behavior; (c) atomic depiction of the scenario in part b; and (d) effect of iodine substitution for sulfur within the structure, leading to n-type character.

uncertainty in the preferred oxidation state thus making empirical accounting nontrivial. In such instances, more precise theoretical calculations may be necessary to account for such behavior. Similar accounting has been used previously in theoretical modeling for II−VI nanoclusters,[27−31] where artificial charging was used to bring the Fermi level of the system to the midgap position, as well as experimentally where a charge neutrality condition of the nanocrystal was imposed for stability.[32,33]

Application to a Model System: PbS CQDs. We now illustrate the oxidation state picture of doping in ionic semiconductors with an example particular to PbS CQDs, highly relevant to photovoltaics, wherein both remote and substitutional doping are expected to impact the free carrier density.

PbS CQDs have been reported to be doped through the use of bound ligands such as thiols or halides.[34−36] In the remote doping configuration (Figure 1a), surface ligands donate charges to the nanocrystal core as a result of band alignments that facilitate charge transfer between the highest occupied molecular orbital (HOMO) of the ligand and the conduction band of the semiconductor nanocrystal. The analogous process can happen for the valence band case as well (Figure 1b), represented in an atomic basis in Figure 1c. The same dopants can also incorporate into the nanocrystal core by replacing lattice atoms as in conventional, bulk semiconductor doping (Figure 1d).

An iodine ion can apparently act as either a p-dopant or an n-dopant depending on whether it is adsorbed (*i.e.*, an increased number of atoms are added into the balance equation), or instead substituted into the lattice (*i.e.*, the number of atoms is conserved, and their identity is altered). In Figure 1c, a stoichiometric PbS CQD is presented with an iodine ion adsorbed on its surface. Using eq 2, adding the iodine ion results in N_{exc} changing to −1, thus a free hole is contributed. Charge neutrality of the system is preserved as the free hole is balanced by the charge of the iodine ion. When instead iodine substitutes for sulfur (Figure 1d), N_{exc} computes to +1, corresponding to an extra electron, that is, n-type doping. This is consistent with experimental observations of iodine being an n-type substitutional dopant in bulk PbS.[37,38]

A comparison of Figure 1 parts c and d shows that the number of sulfur atoms in the originally stoichiometric CQD has changed: thus, it can be seen that the n-type doping achieved in Figure 1d can be predicted simply through counting the number of atoms of each class, without requiring specific tracking of whether substitution was performed. If one more sulfur atom is added on the surface of the dot in Figure 1d to attain the same stoichiometry as in Figure 1c, the same p-type doping would be accomplished.

In sum, tracking the overall stoichiometry of the dot, including all constituent components such as ligands and core dopants, is sufficient to ascertain the net doping. The proposed summation over oxidation states of all constituent atoms fully predicts net doping type and magnitude; n-type for $N_{exc} > 0$, p-type when $N_{exc} < 0$.

DFT Verification of Model. To test these predictions using a more accurate computational framework, we carried out density functional theory (DFT) calculations for PbS CQDs of sizes 1.5−2.4 nm, with different shapes, Pb:S ratios, types, and numbers of ligands. DFT employs a complete basis and ascertains accurate energetic positions and interactions among the orbitals, rather than relying on *a priori* assumptions and knowledge of such energetic relationships as required in the discussion above. Thus DFT calculations provide an objective verification of the proposed picture. In DFT, deviations from the idealized bulk-like structure are also taken into account, such as interstitial dopants, surface reconstructions and self-healing processes,[39,40] each of which can potentially alter the local bonding motifs and oxidation states of the atoms.

The results of this study are summarized in Figure 2a. The figure shows that both the above framework and rigorously evaluated DFT closely predict the same values for N_{exc}. This is true even when the idealized structure of the CQD is disrupted *via* formation of defects and surface reconstructions.

It should be noted that small relative variations in stoichiometry lead to large absolute numbers of excess carriers (tens of electrons per dot) (Figure 2a) corresponding to very high doping densities ($\sim 10^{20}$ cm^{-3}). Increasing the carrier populations in such a manner would be expected to lead to a bleach[13,17,41] of the excitonic transition; however, experimentally, the bleach is rarely seen, an observation explained by the fact that doping also introduces shallow states at the band edges (band tails).[10,16] Indeed, we observe from

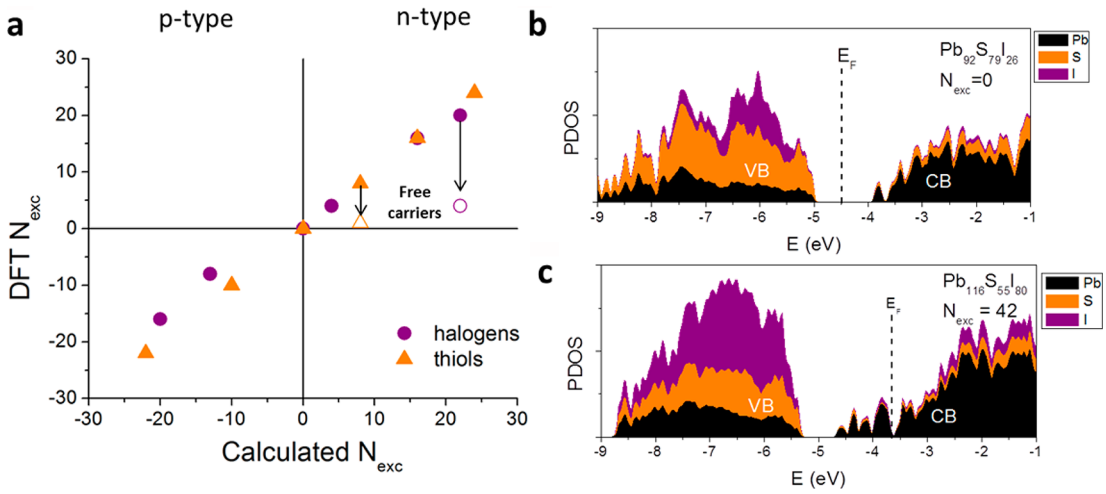

Figure 2. (a) Number of excess electrons evaluated *via* DFT plotted against N_{exc} calculated based on eq 2. Empty shapes indicate the number of nontrapped electrons. (b) DFT projected density of states showing a scenario with a clean bandgap (calculated for a stoichiometric (balanced) quantum dot) and (c) same calculation for a quantum dot with excess Pb, leading to filled gap states near the conduction band and a shift of the Fermi level resulting in n-type behavior. The calculations are for small (~1.8 nm) quantum dots with extreme values of N_{exc} for the purpose of visualization: smaller quantum dots result in more apparent changes in area under the plots to highlight the changes in stoichiometry, stronger shifts in E_F, and noticeable trap states.

DFT that the off-stoichiometry (*i.e.*, nonzero N_{exc} value) does not create truly free carriers along but introduces some number of band tail states that largely consume the extra carriers introduced *via* doping, effectively pinning the Fermi level near the band edge. For several sizes and stoichiometries we carried out a more detailed analysis of the wave functions of the states close to the band edge (Figure 2b,c) in order to track core-like intrinsic states *versus* more surface-localized trap-like states. A preponderance of carriers reside in the introduced surface-like band tail states, while only a small fraction (fewer than 10%) end up as free carriers that contribute to the free carrier density (open symbols in Figure 2a). This picture is consistent with the absence of bleaching observed experimentally in prior reports in spite of high levels of introduced dopants. This type of doping compensation is also a well-known limitation in bulk semiconductors.[42]

Experimental Verification of Model. To verify our charge-orbital balance model and DFT predictions experimentally, we investigated the impact of a number of cationic and anionic treatments on doping type in CQD films. We employed FET test structures to evaluate doping type and magnitude.

We began by investigating a suite of films made from ~3 nm PbS CQDs treated in a rigorously anhydrous environment with halide anions, which previously have been shown to provide robust inorganic passivation.[36] Tetrabutylammonium iodide (TBAI) treated PbS CQD films[43] employed in FETs showed a formation of an n-channel (Figure 3a) capable of shuttling electrons between the drain and the source. In contrast, films treated in an air environment using a strongly oxidizing agent such as tetramethylammonium hydroxide (TMAOH) resulted in the formation of a p-channel (Figure 3b). Other chemical treatments involving various salts and processing environments were employed to yield a complete suite of doping levels as reported by our FET measurements (Figure 3c, Supporting Information, Figure S2). Depending on the chemical treatment and the processing environment, films could be tailored to become n- or p-type and have widely differing majority carrier concentrations.

We desired accurate chemical analysis to obtain stoichiometric information in order to test our charge-orbital balance framework. We observed the quantitative competition among the different species contributing to N_{exc} *via* both RBS and XPS. In each case, the positive and negative contributions were calculated (Figure 4a) based on the preferred oxidation state of each constituent within the film and its relative quantity. The computed N_{exc} (Figure 4b) indicated whether the material was expected to be n-type or p-type ($N_{exc} > 0$ predicting n-type, $N_{exc} < 0$ predicting p-type). The doping type predictions were consistent with observed FET results.

Model Application: Reversible Switching of Doping Type. We explored further the role of oxygen in CQD films—perhaps the most widely deployed (deliberately or not) CQD film dopant. Oxygen is a known acceptor in PbS[44] and can readily overwhelm n-type doping implemented in inert environment processing. We took TBAI-treated, n-type films (Figure 5a) and further treated using amines. The amines, L-type ligands as noted above, are expected to make no net contribution in the charge-orbital balance picture.[45] It was therefore an initial surprise that p-type doping was observed after (Figure 3c, Figure 5b) amine treatment. We carried

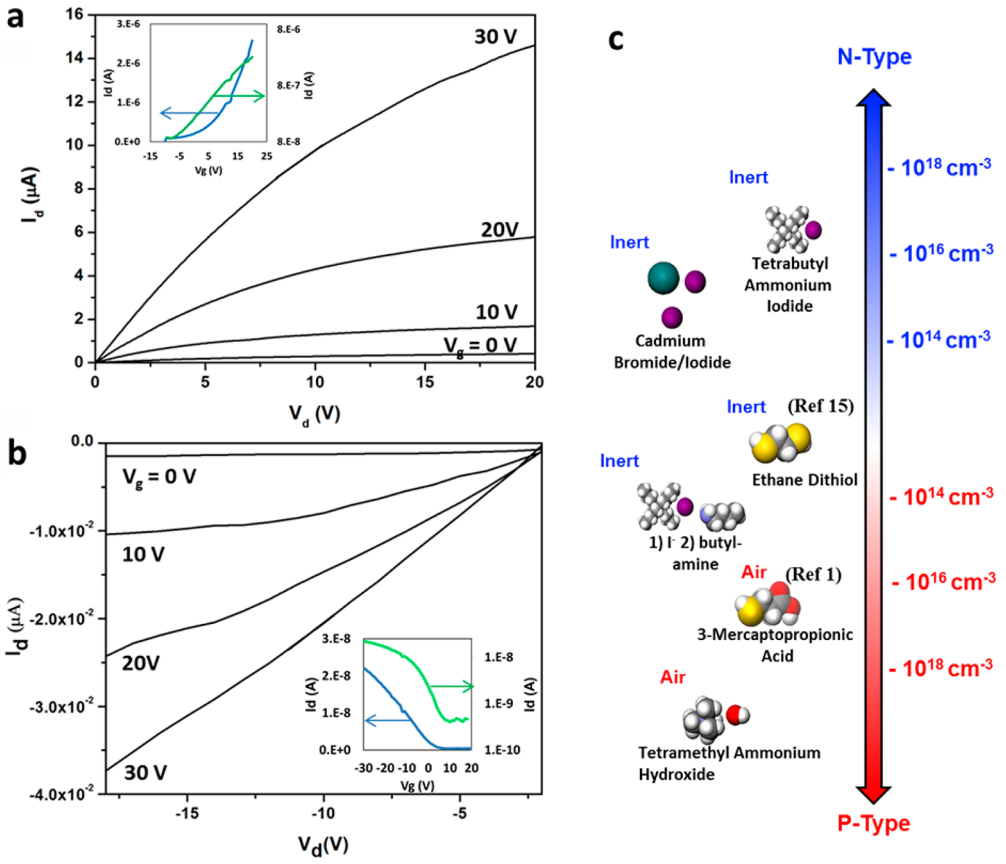

Figure 3. (a) FET output characteristics of TBAI-treated PbS CQD films (inset: transfer curve) showing n-type response. (b) FET output characteristics of TMAOH-treated PbS CQD films (inset: transfer curve) showing p-type response. (c) Illustration of the effect of various treatments of PbS CQD films conducted under various atmospheres (shown on the left) on the doping density (shown on the right).

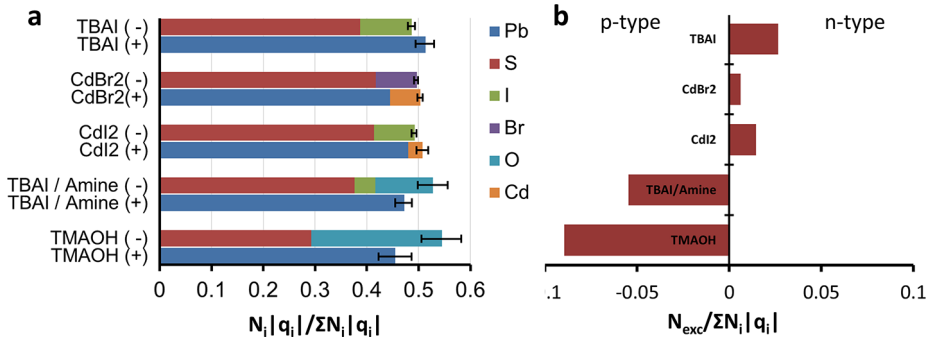

Figure 4. (a) Normalized positive and negative contributions to N_{exc} from specific atomic species and molecules. (b) Overall N_{exc} value calculated to show if a material is expected to be n-type or p-type.

out RBS and XPS analyses and found that a significant quantity of iodine had been displaced from the film while the amount of sulfur was unchanged (Figure 5d), which should further move the film toward n-type according to eq 2. It was also evident that upon exposure of a TBAI film to amines, a significant increase in oxygen concentration was observed. We interpret these results to indicate that the amine treatment had removed a substantial amount of halides, making the CQD surface highly reactive, and thereby allowed the small level of residual oxygen inside the glovebox environment to react with the CQDs' now-exposed surfaces. Since oxygen enters eq 2 with an oxidation state of −2, it can move CQD toward being p-type at double the rate-per-species compared with typical monovalent ligands (oxidation state of −1). These two factors combined—exposure of the surface resulting from iodide ion removal, leading to high reactivity, combined with the high oxidation number of oxygen—ensure that oxygen's p-doping effect outcompetes the contribution of the excess cations that provide the opposite propensity toward n-typeness (Figure 4). In all cases, subsequent iodide retreatment, which we found removed the oxygen (S3), returned

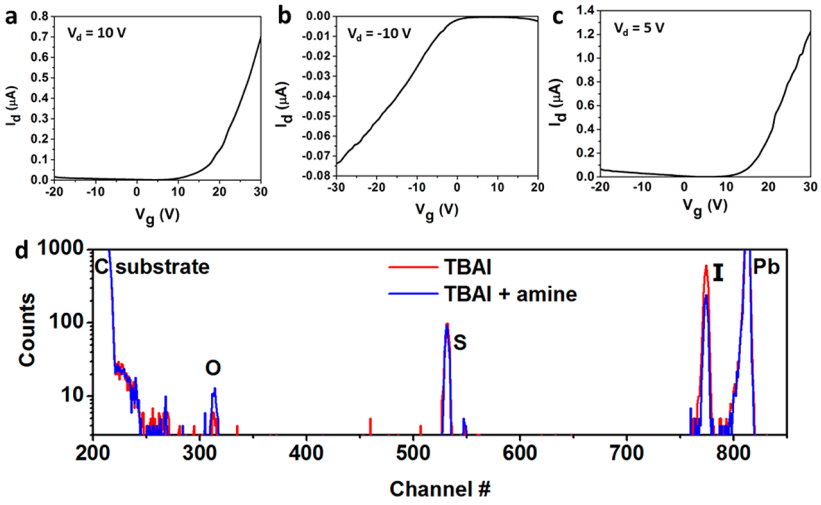

Figure 5. (a) n-type TBAI-treated CQD FET transfer curve. (b) FET transfer curve for the same CQD film after treatment with butylamine shows p-type behavior. (c) FET transfer curve for the same CQD film after retreating with iodine ions shows a reversal of the character back to n-type, and (d) RBS spectra showing oxygen and iodine content for panels a (red) and b (blue).

the film to n-type (Figure 5c). The charge−orbital balance model, coupled with compositional analysis techniques, provided a self-consistent and predictive framework for the doping-type switching behavior facilitated by oxygen.

CONCLUSIONS

The present work provides a framework—validated using both modeling and experiment—to predict doping in CQD films. The framework predicts the majority carrier type of the films and does so based solely on stoichiometry. The origins of the picture lie in the principle of charge−orbital balance. In CQD systems, off-balance stoichiometry in the core strongly contributes to the doping type, and this effect can easily dominate over the impact of chemical treatments and rational dopants introduced during synthesis. Both remote dopants and substitutional impurities are consolidated under this single framework, offering a unified path toward realizing predictably doped CQD solids. The work paves the way for the engineering of novel CQD materials with a variety of dopants and carrier densities. Such versatility will allow for CQD films to be used in advanced optoelectronic devices such as bipolar transistors, thyristors, and multijunction devices which require both n-type and p-type materials.

METHODS

Materials Preparation. PbS CQDs of ∼3 nm are fabricated following a published recipe.[36,46]

Film Deposition. Layer-by-layer (LBL) spin-casting was applied to fabricate the CQD films. Treatments were done in inert or air ambient environment. Ligands were dissolved in methanol at 10 mg mL^{-1}. The fabrication process consisted of the following steps: (1) 2 drops of PbS CQDs in octane (25 mg mL^{-1}) were dropped onto substrates and were spin-cast at 2500 rpm for 10 s; (2) 0.75 mL of ligand solution was deposited, followed by spin-casting for 10 s at 2500 rpm; (3) 0.75 mL of methanol was dropped and spin-cast at 2500 rpm for 10 s (repeat twice). Steps 1−3 were repeated until the desired thickness of PbS CQDs films was reached.

XPS Characterization. The surface elements and chemical states of PbS CQDs were examined using X-ray photoelectron spectroscopy (XPS, PHI-5500) with a monochromated Al Kα radiation source (1486.7 eV) to excite photoelectrons in an ultrahigh vacuum atmosphere at $\sim 10^{-9}$ Torr. XPS was carried out to qualitatively confirm the RBS findings; however, we believe RBS values to be more accurate and thus used in Figure 4.

RBS Characterization. Measurements were performed at the Tandetron facility at the University of Western Ontario. The films (1−4 LBL) were spin-cast on diamond-like carbon or Si substrates. Measurements were done at 2.5, 3.7, and 4.5 MeV beam energies and average stoichiometry values are reported in the text. Channel-energy calibration was performed using a Si standard with a surface layer δ-doped with Sb. Fits of integrated count plots, accounting for atomic sensitivity factors and the deposited layer densities and thicknesses, were performed with the SIMNRA software.[47]

FET Measurement. Commercial silicon wafers (highly doped p-type using boron) with a thin layer of thermally oxidized SiO_2 were used as substrates and gate dielectric. Au and Al (or Ag) were used as the source and drain electrodes to form the ohmic contact to p-type and n-type materials, respectively. For bottom-contacted FET studies, prepatterned Au contacts were used with a channel length of 5 μm and channel width of 1 mm. Top-contacted FET devices employed thermal evaporation of Al or Ag through a shadow mask to create channel lengths of 25 and 50 μm and channel widths of 500 and 100 μm. A typical CQD film thickness for FET studies was 40 nm. FET measurements were performed inside an N_2-glovebox. The FET structures used to measure the CdI_2 and $CdBr_2$ treated films employed a high ε gate dielectric. These were made by PVD of Al onto a glass substrate, followed by electrochemical anodization to form an 8 nm gate oxide. Octadecyl trichlorosilane was used as a passivating surfactant. The films were prepared by spin coating and solid state ligand exchange. Titanium was employed as the top contact. The completed FET device had a channel length of 33 μm and a channel width of 2 mm.

DFT Calculations. DFT simulations were performed using the SIESTA software[48] based on pseudopotentials and numerical atomic orbitals as a basis. The generalized gradient approximation

with PBE96 exchange-correlation was used throughout. Scalar-relativistic Troullier–Martins pseudopotentials with nonlinear core corrections were used. Charge density was represented on a grid with at least 200 Ry cutoff and the GridCellSampling option to effectively double the cutoff for better convergence of forces on atoms. Geometry optimizations were performed until the forces on the atoms converged to below 40 meV/A.

Conflict of Interest: The authors declare no competing financial interest.

Supporting Information Available: Orbital filling example, additional FET transfer curves, and RBS spectra. This material is available free of charge *via* the Internet at http://pubs.acs.org.

Acknowledgment. This publication is based in part on work supported by Award KUS-11-009-21, made by King Abdullah University of Science and Technology (KAUST), by the Ontario Research Fund Research Excellence Program, and by the Natural Sciences and Engineering Research Council (NSERC) of Canada. David Zhitomirsky would like to acknowledge his NSERC CGS D scholarship. We thank Angstrom Engineering, Inc. and Innovative Technology, Inc. for useful discussions regarding material deposition methods and control of the glovebox environment, respectively. We thank Lyudmila Goncharova for help in RBS measurements and Mark Greiner for help in XPS measurements. We thank Larissa Levina for PbS CQD synthesis and Melissa Furukawa for FET measurements. Computations were performed on the GPC supercomputer at the SciNet[49] HPC Consortium. SciNet is funded by the Canada Foundation for Innovation under the auspices of Compute Canada, the Government of Ontario, Ontario Research Fund–Research Excellence, and the University of Toronto.

REFERENCES AND NOTES

1. Pattantyus-Abraham, A. G.; Kramer, I. J.; Barkhouse, A. R.; Wang, X.; Konstantatos, G.; Debnath, R.; Levina, L.; Raabe, I.; Nazeeruddin, M. K.; Gratzel, M.; *et al.* Depleted-Heterojunction Colloidal Quantum Dot Solar Cells. *ACS Nano* **2010**, *4*, 3374–3380.
2. Li, Y. Q.; Rizzo, A.; Cingolani, R.; Gigli, G. Bright White-Light-Emitting Device from Ternary Nanocrystal Composites. *Adv. Mater.* **2006**, *18*, 2545–2548.
3. Geyer, S. M.; Allen, P. M.; Chang, L.-Y.; Wong, C. R.; Osedach, T. P.; Zhao, N.; Bulovic, V.; Bawendi, M. G. Control of the Carrier Type in InAs Nanocrystal Films by Predeposition Incorporation of Cd. *ACS Nano* **2010**, *4*, 7373–7378.
4. Caruge, J. M.; Halpert, J. E.; Wood, V.; Bulovic, V.; Bawendi, M. G. Colloidal Quantum-Dot Light-Emitting Diodes with Metal-Oxide Charge Transport Layers. *Nat. Photon.* **2008**, *2*, 247–250.
5. Luther, J. M.; Law, M.; Beard, M. C.; Song, Q.; Reese, M. O.; Ellingson, R. J.; Nozik, A. J. Schottky Solar Cells Based on Colloidal Nanocrystal Films. *Nano Lett.* **2008**, *8*, 3488–3492.
6. Ma, W.; Luther, J. M.; Zheng, H.; Wu, Y.; Alivisatos, A. P. Photovoltaic Devices Employing Ternary PbS_xSe_{1-x} Nanocrystals. *Nano Lett.* **2009**, *9*, 1699–1703.
7. Pearson, G. L.; Bardeen, J. Electrical Properties of Pure Silicon and Silicon Alloys Containing Boron and Phosphorus. *Phys. Rev.* **1949**, *75*, 865–883.
8. Kohn, W. Shallow Impurity States in Silicon and Germanium. *Solid State Physics* **1957**, *5*, 257–320.
9. Shockley, W.; Queisser, H. J. Detailed Balance Limit of Efficiency of p-n Junction Solar Cells. *J. Appl. Phys.* **1961**, *32*, 510–519.
10. Talapin, D. V.; Murray, C. B. PbSe Nanocrystal Solids for n- and p-Channel Thin Film Field-Effect Transistors. *Science* **2005**, *310*, 86–89.
11. Sahu, A.; Kang, M. S.; Kompch, A.; Notthoff, C.; Wills, A. W.; Deng, D.; Winterer, M.; Frisbie, C. D.; Norris, D. J. Electronic Impurity Doping in CdSe Nanocrystals. *Nano Lett.* **2012**, *12*, 2587–2594.
12. Choi, J.-H.; Fafarman, A. T.; Oh, S. J.; Ko, D.-K.; Kim, D. K.; Diroll, B. T.; Muramoto, S.; Gillen, J. G.; Murray, C. B.; Kagan, C. R. Bandlike Transport in Strongly Coupled and Doped Quantum Dot Solids: A Route to High-Performance Thin-Film Electronics. *Nano Lett.* **2012**, *12*, 2631–2638.
13. Shim, M.; Guyot-Sionnest, P. N-Type Colloidal Semiconductor Nanocrystals. *Nature* **2000**, *407*, 981–983.
14. Nag, A.; Chung, D. S.; Dolzhnikov, D. S.; Dimitrijevic, N. M.; Chattopadhyay, S.; Shibata, T.; Talapin, D. V. The Effect of Metal Ions on Photoluminescence, Charge Transport, Magnetic and Catalytic Properties of All-Inorganic Colloidal Nanocrystals and Nanocrystal Solids. *J. Am. Chem. Soc.* **2012**, *134*, 13604–13615.
15. Norris, D. J.; Efros, A. L.; Erwin, S. C. Doped Nanocrystals. *Science* **2008**, *319*, 1776 –1779.
16. Mocatta, D.; Cohen, G.; Schattner, J.; Millo, O.; Rabani, E.; Banin, U. Heavily Doped Semiconductor Nanocrystal Quantum Dots. *Science* **2011**, *332*, 77–81.
17. Liu, H.; Keuleyan, S.; Guyot-Sionnest, P. N- and p-Type HgTe Quantum Dot Films. *J. Phys. Chem. C* **2011**, *116*, 1344–1349.
18. Osedach, T. P.; Zhao, N.; Andrew, T. L.; Brown, P. R.; Wanger, D. D.; Strasfeld, D. B.; Chang, L.-Y.; Bawendi, M. G.; Bulović, V. Bias-Stress Effect in 1,2-Ethanedithiol-Treated PbS Quantum Dot Field-Effect Transistors. *ACS Nano* **2012**, *6*, 3121–3127.
19. Murrel, J. N.; Kettle, S. F.; Tedder, J. M. *The Chemical Bond*, 2nd ed.; John Wiley and Sons: New York, 1985.
20. An, J. M.; Franceschetti, A.; Dudiy, S. V.; Zunger, A. The Peculiar Electronic Structure of PbSe Quantum Dots. *Nano Lett.* **2006**, *6*, 2728–2735.
21. Boguslawski, P.; Gorczyca, I. Atomic-Orbital Interpretation of Electronic Structure of III–V Semiconductors: GaAs *versus* AlAs. *Semicond. Sci. Technol.* **1994**, *9*, 2169.
22. Hoffmann, R. A Chemical and Theoretical Way To Look at Bonding on Surfaces. *Rev. Mod. Phys.* **1988**, *60*, 601–628.
23. Sze, S. *Physics of Semiconductor Devices*; Wiley: New York, 1981.
24. Mavros, M. G.; Micha, D. A.; Kilin, D. S. Optical Properties of Doped Silicon Quantum Dots with Crystalline and Amorphous Structures. *J. Phys. Chem. C* **2011**, *115*, 19529–19537.
25. Fischer, S. A.; Prezhdo, O. V. Dopant Effects on Single and Multiple Excitons in Small Si Clusters: High-Level *ab Initio* Calculations. *J. Phys. Chem. C* **2011**, *115*, 10006–10011.
26. Kilina, S.; Velizhanin, K. A.; Ivanov, S.; Prezhdo, O. V.; Tretiak, S. Surface Ligands Increase Photoexcitation Relaxation Rates in CdSe Quantum Dots. *ACS Nano* **2012**, *6*, 6515–6524.
27. Gurin, V. S. A Variety of Metal Chalcogenide Clusters: MOLCAO Calculations and Interplay between Quantum-Sized Semiconductors and Multinuclear Complexes. *Colloids Surf., A* **2002**, *202*, 215–222.
28. Lee, G. S. H.; Craig, D. C.; Ma, I.; Scudder, M. L.; Bailey, T. D.; Dance, I. G. $[S_4Cd_{17}(SPh)_{28}]^{2-}$, the First Member of a Third Series of Tetrahedral $[S_wM_x(SR)_y]^{z-}$ Clusters. *J. Am. Chem. Soc.* **1988**, *110*, 4863–4864.
29. Frenzel, J.; Joswig, J.-O.; Seifert, G. Optical Excitations in Cadmium Sulfide Nanoparticles. *J. Phys. Chem. C* **2007**, *111*, 10761–10770.
30. Voznyy, O. Mobile Surface Traps in CdSe Nanocrystals with Carboxylic Acid Ligands. *J. Phys. Chem. C* **2011**, *115*, 15927–15932.
31. Feng, P.; Bu, X.; Zheng, N. The Interface Chemistry Between Chalcogenide Clusters and Open Framework Chalcogenides. *Acc. Chem. Res.* **2004**, *38*, 293–303.
32. Moreels, I.; Justo, Y.; Geyter, B.; De; Haustraete, K.; Martins, J. C.; Hens, Z. Size-Tunable, Bright, and Stable PbS Quantum Dots: A Surface Chemistry Study. *ACS Nano* **2011**, *5*, 2004–2012.
33. Fritzinger, B.; Capek, R. K.; Lambert, K.; Martins, J. C.; Hens, Z. Utilizing Self-Exchange To Address the Binding of Carboxylic Acid Ligands to CdSe Quantum Dots. *J. Am. Chem. Soc.* **2010**, *132*, 10195–10201.
34. Gao, J.; Luther, J. M.; Semonin, O. E.; Ellingson, R. J.; Nozik, A. J.; Beard, M. C. Quantum Dot Size Dependent *J–V* Characteristics in Heterojunction ZnO/PbS Quantum Dot Solar Cells. *Nano Lett.* **2011**, *11*, 1002–1008.

35. Leschkies, K. S.; Beatty, T. J.; Kang, M. S.; Norris, D. J.; Aydil, E. S. Solar Cells Based on Junctions between Colloidal PbSe Nanocrystals and Thin ZnO Films. *ACS Nano* **2009**, *3*, 3638–3648.
36. Tang, J.; Kemp, K. W.; Hoogland, S.; Jeong, K. S.; Liu, H.; Levina, L.; Furukawa, M.; Wang, X.; Debnath, R.; Cha, D.; *et al*. Colloidal-Quantum-Dot Photovoltaics Using Atomic-Ligand Passivation. *Nat. Mater.* **2011**, *10*, 765–771.
37. Kwan, S. H.; Colozzi, C. G.; Linz, A. Halogen Vapor-Deposition of Chalcogenide Crystals—Lead Sulfide. *J. Appl. Phys.* **1974**, 3273–3276.
38. Peng, H.; Song, J.-H.; Kanatzidis, M. G.; Freeman, A. J. Electronic Structure and Transport Properties of Doped PbSe. *Phys. Rev. B* **2011**, *84*, 125207.
39. Puzder, A.; Williamson, A. J.; Gygi, F.; Galli, G. Self-Healing of CdSe Nanocrystals: First-Principles Calculations. *Phys. Rev. Lett.* **2004**, *92*, 217401.
40. Yu, M.; Fernando, G. W.; Li, R.; Papadimitrakopoulos, F.; Shi, N.; Ramprasad, R. First Principles Study of CdSe Quantum Dots: Stability, Surface Unsaturations, and Experimental Validation. *Appl. Phys. Lett.* **2006**, *88*, 231910–3.
41. Yu, D.; Wang, C.; Guyot-Sionnest, P. n-Type Conducting CdSe Nanocrystal Solids. *Science* **2003**, *300*, 1277–1280.
42. Zunger, A. Practical Doping Principles. *Appl. Phys. Lett.* **2003**, *83*, 57–59.
43. Zhitomirsky, D.; Furukawa, M.; Tang, J.; Sadler, P.; Hoogland, S.; Voznyy, O.; Liu, H.; Sargent, E. H. N-Type Colloidal Quantum Dot Solids for Photovoltaics. *Adv. Mater.* **2012**, DOI:10.1002/adma.201202825.
44. Harada, R. H.; Minden, H. T. Photosensitization of PbS Films. *Phys. Rev.* **1956**, *102*, 1258–1262.
45. Kutana, A.; Erwin, S. C. PbSe Nanocrystals Remain Intrinsic after Surface Adsorption of Hydrazine. *Phys. Rev. B* **2011**, *83*, 235419.
46. Hines, M. A.; Scholes, G. D. Colloidal PbS Nanocrystals with Size-Tunable Near-Infrared Emission: Observation of Post-Synthesis Self-Narrowing of the Particle Size Distribution. *Adv. Mater.* **2003**, *15*, 1844–1849.
47. Mayer, M. SIMNRA, A Simulation Program for the Analysis of NRA, RBS, and ERDA. *AIP Conf. Proc.* **1999**, *475*, 541–544.
48. Soler, J. M.; Artacho, E.; Gale, J. D.; García, A.; Junquera, J.; Ordejón, P.; Sánchez-Portal, D. The SIESTA Method for *ab Initio* Order-N Materials Simulation. *J. Phys.: Condens. Matter.* **2002**, *14*, 2745.
49. Loken, C.; Gruner, D.; Groer, L.; Peltier, R.; Bunn, N.; Craig, M.; Henriques, T.; Dempsey, J.; Yu, C.-H.; Chen, J.; *et al*. SciNet: Lessons Learned from Building a Power-Efficient Top-20 System and Data Centre. *J. Phys.: Conf. Ser.* **2010**, *256*, 012026.